Diagnostics for Periodically Excited Actuators

Łukasz Huchel, Jan Helsen, Peter A. Lindahl, and Steven B. Leeb

***Abstract*— Electromechanical actuators that operate cyclically or with periodically varying loads present unique opportunities for condition-based diagnostics. Signal processing techniques can be tailored to exploit periodic variation in the electrical and mechanical variables and waveforms associated with these machines. These analytical techniques improve signal resolution and permit detection of fine changes in system parameters. This article presents low-intrusion instrumentation tailored to periodic loads. These instruments can provide subtle diagnostic information from measurements of quantities such as vibration and electrical current. Extraction of cyclostationary signal components and development of diagnostic metrics are discussed in this article and demonstrated on an industrially relevant case, a diaphragm pump.**

***Index Terms*— Cyclostationarity, diaphragm pump, instrumentation and diagnostics, spectral correlation, switched capacitor filter.**

I. Introduction

ELECTROMECHANICAL actuators with periodically varying loads serve as workhorse components in many industrial and commercial processes [1]–[4]. Compressors for heating, ventilation, and air conditioning (HVAC) and high-pressure air service, machine tools with periodic stamping or cutting, and reciprocating pumps all experience periodic load variations throughout a mechanical operating cycle [5], [6]. Associated periodic modulations appear in many signals associated with these actuators and machines, including vibration, electrical current, speed, and torque [6], [7]. These periodic variations are an underexploited opportunity for diagnostics. Signal processing techniques and measurement hardware can be tailored to exploit periodic signal features that enhance measurement accuracy [8] and the possibilities for fault detection [9]–[12]. This article introduces a combination of adaptive filtering and sampling hardware combined with signal processing methods to create fault detection and diagnostic metrics for electromechanical actuators with periodically varying loads. The combined hardware and software techniques offer an instrumentation and measurement system tailored to utilize unique features of periodically excited actuators.

Diaphragm pumps are one example of an industrially important, periodically cycling actuator. These pumps are critical for many medical, food, and petrochemical processes [13], [14], as they offer volumetric precision, high discharge pressures, and superior isolation of the working fluid. Diaphragm pumps also exhibit significant failure mechanisms. Two main challenges reported in the literature include diaphragm rupture and check valve failure [15], [16]. These two phenomena are related. For example, inlet valve clogging can lead to premature diaphragm damage. Physical rupture of the diaphragm can lead to contamination of the process liquids by hydraulic oil from the pump's mechanism.

There are a relatively few publications that examine the analytical description of diaphragm pump operation and associated degradation in practical environments [15], [17], e.g., in comparison to centrifugal pumps. Moreover, a few references deal with diagnostics and condition monitoring of these positive displacement devices [18]–[20]. Diaphragm pumps are susceptible to several crippling failure mechanisms and are often employed in harsh environments that induce regular degradation and eventual failure. The focus of this article will be fault detection for diaphragm pumps. The techniques developed here apply to other periodically cycled actuators, e.g., compressors and stamping machine tools.

New hardware and associated signal processing techniques that exploit the inherent periodic excitation in these types of loads will be demonstrated analyzing a LEWA EK-1 diaphragm pump [21]. Among other benefits, these signal processing techniques utilize periodicity to reduce the need for transmitting or storing large quantities of sampled data. Cyclically aware signal processing algorithms focus on signal features relevant to diagnostics, and, with appropriate instrumentation hardware, are ideal for remote or embedded diagnostic systems [22]. That is, awareness of periodic operation makes it easier to create actionable diagnostic indicators right "at the edge" of the sensing environment.

II. Diagnostic Approach

Periodic operation colors or impacts the structure of many different physical signals associated with an actuator. For example, periodic variations may appear in torque, current, vibration, acoustic signature, and other signals. Diagnostics indicators are often found in many or all of these signals. Some may be easier or more appropriate to measure in a given application. For example, where control requires current sensing, current measurements may be available without the

Manuscript received June 24, 2019; revised August 28, 2019; accepted October 1, 2019. Date of publication October 18, 2019; date of current version June 9, 2020. This work was supported in part by the MITEI-ExxonMobil Initiative, in part by the ONR Structural Acoustic Program, and in part by the Fulbright Foundation. The Associate Editor coordinating the review process was Zhigang Liu. *(Corresponding author: Łukasz Huchel.)*

Ł. Huchel, P. A. Lindahl, and S. B. Leeb are with the Department of Electrical Engineering and Computer Science, Massachusetts Institute of Technology, Cambridge, MA 02139 USA (e-mail: lhuchel@mit.edu; lindahl@mit.edu; sbleeb@mit.edu).

J. Helsen is with the OWI-Lab, Vrije Universiteit Brussel, 1050 Brussel, Belgium (e-mail: jan.helsen@vub.be).

Color versions of one or more of the figures in this article are available online at http://ieeexplore.ieee.org.

Digital Object Identifier 10.1109/TIM.2019.2947971

added expense. On the other hand, sealed or electrically isolated or installed systems may be more easily analyzed from mechanical measurements. The sections below describe two illustrative approaches, one examining the cyclostationary components of a vibration signature, and the second examining frequency components of a current signal associated with the induction machine driving the device under study.

A. Cyclostationary Vibration Components

Alternating suction and discharge cycles create a nonuniform loading condition over a single operating cycle of a diaphragm pump. The pump's head acceleration is influenced by these cyclic variations, which results in a strongly modulated vibration signal. Detection of variations and subtle periodicity in a signal can be challenging for conventional spectral analysis techniques [23]. For example, random content can interfere with the detection and isolation of the periodic part of a signal [24]. Antoni [4] shows examples targeted to a diesel engine and a centrifugal pump, and highlights how inspection of the power spectral density can fail to distinguish hidden periodicity in the vibration signals.

The concept of cyclostationarity can be used to expose the impact of load torque modulation on vibration measurements. Informally, cyclostationarity extends the class of stationary signals to signals with periodically changing statistical properties [25]. Mechanically, cyclostationary signals can arise from periodic modulations of multiple modes of motion, for example, as in a musical instrument. Formally, a signal is said to exhibit cyclostationarity if a particular cascade of linear and nonlinear transformations reveal periodic components or information content in the signal [26]. Certain classes of operations are typical. For example, associated linear operations include a filtering operation, while nonlinear transforms might be applied in the form of a squaring operator, $|\ |^2$.

A "spectral correlation" function [23] can be used to isolate and detect cyclostationary components in a vibration signal. The spectral correlation function defines a set of spectral coefficients

$$S_x(\alpha, f) = \int_{-\infty}^{\infty} R_x^{\alpha}(\tau) e^{-j2\pi f \tau} d\tau \tag{1}$$

where R_x^{α} represents a cyclic autocorrelation function.

$$R_x^{\alpha}(\tau) = \frac{1}{T} \int_{-\frac{T}{2}}^{\frac{T}{2}} R_x(t, \tau) e^{-j2\pi \alpha t} dt \tag{2}$$

The cyclic autocorrelation function can be interpreted as the Fourier series coefficients of an autocorrelation function $R_x(t, \tau)$, defined as:

$$R_x(t, \tau) = \mathbb{E}[x(t)x^*(t - \tau)] \tag{3}$$

where $\mathbb{E}$ stands for an ensemble average. For the ergodic processes, (3) can be estimated with the time average operator [27]. The variable $x(t)$ is the signal to be analyzed, e.g., a vibration signal; α is a cyclic or modulation frequency; f is a carrier frequency, e.g., the average speed or vibration frequency of the pump; and T is a measurement interval. Spectral correlation coefficients in (1) describe the energy distribution across both cyclic frequency α and carrier frequency f. In the special case of $\alpha = 0$ and stationary signal $x(t)$, (1) is simply a power spectral density function [24]. Discrete-time formulation of (1) is given in the Appendix.

Given a time-domain signal $x(t)$, spectral correlation function can be defined as in (1)–(3). The spectral correlation coefficients can also be understood from the frequency transform of the time-domain signal. For example, we can define the short-time Fourier transform [24] of $x(t)$ as

$$X_{\Delta f}(t, f) = \int_{t-\frac{1}{2\Delta f}}^{t+\frac{1}{2\Delta f}} x(v) e^{-j2\pi f v} dv \tag{4}$$

where Δf is the bandwidth around frequency component f. Gardner [28] demonstrates that $S_x(\alpha, f)$ can be obtained with the correlation of the frequency transforms, as in

$$S_x(\alpha, f) = \lim_{\Delta f \to 0} \lim_{T \to \infty} \frac{\Delta f}{T} \int_{-\frac{T}{2}}^{\frac{T}{2}} [X_{\Delta f}(t, f) X_{\Delta f}^*(t, f + \alpha)] dt \tag{5}$$

where base of this observation are properties of the cross-spectral density. Inspection of (4) and (5) shows that the spectral correlation function is a measure of temporal correlation between the complex envelopes evaluated at f and $f + \alpha$.

The spectral correlation function provides the promising capability of detecting modulation components in an environment with low signal-to-noise ratio (SNR) [23]. When $x(t)$ is a stationary random signal without cyclostationarity, (1) is essentially zero for all $\alpha \neq 0$, a result of the time-shift property of the autocorrelation sequence applied to a stationary signal. The spectral correlation coefficients, therefore, reject possible noise and interference. A conventional approach with $\alpha = 0$ fails to reject the impact of interfering stationary noise.

As an estimator of the spectral correlation, the fast spectral correlation is used [26]. The MATLAB implementation of the fast spectral correlation is available in [29]. In order to mitigate scaling effects and allow for a reliable comparison between estimates of the spectral correlation, it is recommended to normalize the estimate [4], [10]. The spectral correlation is normalized by the square root of power spectral density evaluated at both frequencies: f and $f + \alpha$. This unitless quantity is commonly referred to as the spectral coherence $\gamma_x(\alpha, f)$

$$\gamma_x(\alpha, f) = \frac{S_x(\alpha, f)}{\sqrt{S_x(0, f) S_x(0, f + \alpha)}}. \tag{6}$$

This spectral coherence is effectively normalized for the background signal and noise floor for a signal of interest. We develop a new figure-of-merit for the spectral content by integrating over a carrier frequency range F for any particular choice of α. This figure-of-merit, the mean envelope spectrum (MES), summarizes the average impact of modulating frequency component α on carrier frequencies f in the range of F

$$S_{\mathbf{m}x}(\alpha) = \frac{1}{|F|} \int_F |\gamma_x(\alpha, f)| df. \tag{7}$$

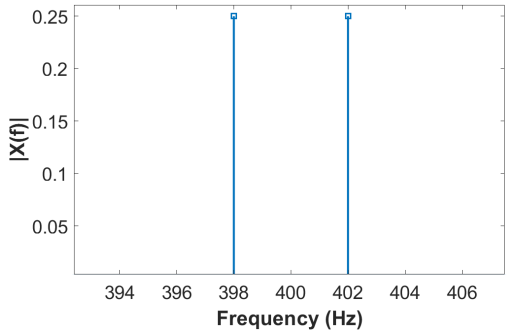

Fig. 1. Magnitude frequency spectrum of the deterministic signal.

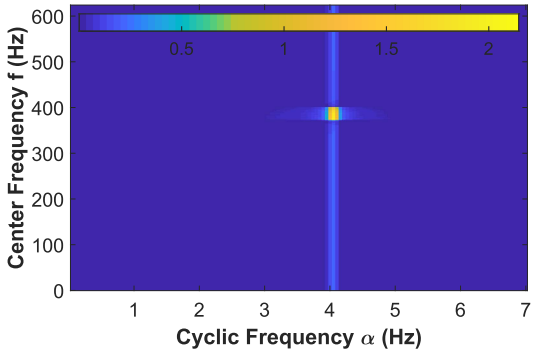

Fig. 2. Spectral coherence map of the deterministic signal.

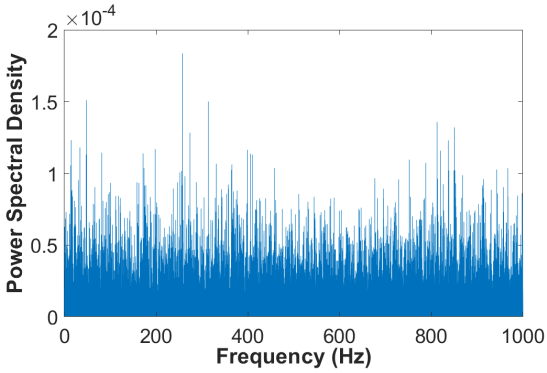

Fig. 3. Power spectral density of the random signal.

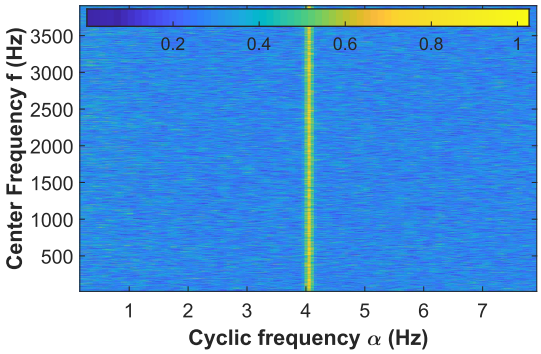

Fig. 4. Spectral coherence map of the random signal.

To illustrate the properties of the spectral correlation, consider a signal

$$x(t) = \cos\left(2\pi\left(f + \frac{\alpha}{2}\right)t\right)\cos\left(2\pi\frac{\alpha}{2}t\right) = \frac{1}{4}(e^{j2\pi(f+\alpha)t} + e^{j2\pi ft} + e^{-j2\pi(f+\alpha)t} + e^{-j2\pi ft}) \quad (8)$$

where $(\alpha/2) = 2$ Hz and $f + (\alpha/2) = 400$ Hz. Figs. 1 and 2 show the positive frequency magnitude spectrum and the spectral coherence map, respectively, for the signal in (8). As expected by inspection of (8), the spacing of the frequency components in the frequency domain is equal to $\alpha = 4$ Hz. As expected from (5), the temporal correlation of $X_{\Delta f}(t, f)$ sequence with $X_{\Delta f}(t, f + \alpha)$ sequence reveals a component at $f = 398$ Hz and $\alpha = 4$ Hz on the spectral coherence map.

Next, consider a random signal that consists of a carrier modulated by a low-frequency signal

$$x(t) = x_{\mathbf{t}}\cos(2\pi 2t) \quad (9)$$

where $x_{\mathbf{t}}$ is a value of a random variable with Gaussian probability density function, zero mean, and unity variance. Figs. 3 and 4 present the power spectral density and spectral coherence, respectively. It can be observed that the power spectral density fails to recognize the periodic variations in the signal of interest. The power spectral density is essentially wideband. However, the spectral coherence map gives a very clear indication of a periodicity. The random nature of the carrier is manifested by the presence of vertical line across all carrier frequencies f.

B. Spectral Current and Vibration Components

The first approach to fault detection and diagnostics uses current signature analysis associated with an induction machine driving the device under study [6], [11]. Experimental results confirm that the fundamental component of a current signal provides little diagnostic information. Moreover, it often masks subtle components that tend to be useful for diagnostic purposes. A custom adaptive discrete-time notch filter in our hardware is used to remove the fundamental component of the current signal and enhance opportunities for diagnostics.

The second approach monitors the energy level at one of the mechanical resonances of the pump's head structure. The acceleration measured at the pump's head is used to extract the desired information. Both diaphragm degradation and inlet valve clogging significantly impact the energy level at this resonant frequency. An impulse response decay analysis is able to identify the spectral location of the resonance. A sensitivity study for the location of the resonant frequency was performed to understand and minimize the influence of different mounting conditions of the diaphragm pump. An example of the acceleration signal acquired using the industrial integrated electronic piezoelectric (IEPE) sensor during the decay experiment is shown in Fig. 5. The signal shown in Fig. 5 is the response of the LEWA EK-1 industrial pump.

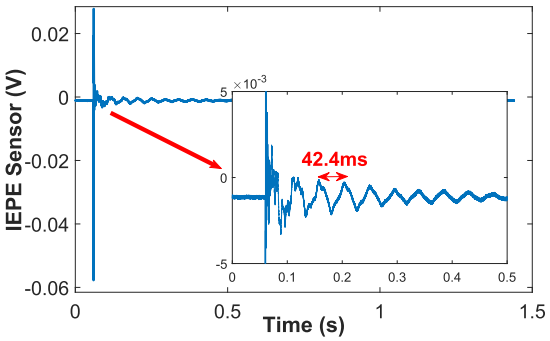

Fig. 5. IEPE sensor data during a natural response.

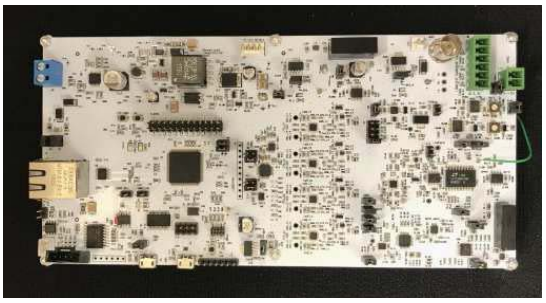

Fig. 6. Custom data acquisition board.

III. Experimental Setup

A custom data acquisition system was developed to permit focus on modulating signals most relevant for the device diagnostics. Validation of the diagnostic strategies was performed on a high-pressure setup emulating a work environment of a diaphragm pump.

A. Acquisition Hardware

The custom data acquisition system provides four simultaneously acquired channels with a resolution of 24 b and a sampling frequency up to 64 kHz. Data can be stored locally or accessed remotely via a 100 Mb/s Ethernet connection which can simultaneously power the device via Power over Ethernet technology. The data acquisition board shown in Fig. 6 is equipped with a dedicated active filter for current signal processing. The adaptive discrete-time notch filter is implemented with two stages of an LTC1060 switched capacitor filter IC. The bandwidth is fixed by the hardware configuration, while the center frequency is adapted. Firmware is responsible for tracking the fundamental frequency variations and updating the center frequency. This discrete-time switched capacitor filter is used for fundamental frequency rejection in the current signal.

As shown in Fig. 7, the system includes a custom feedback loop to continuously adapt the filter center frequency depending on the fundamental frequency of a power source. That is, as the utility supplying an induction machine or another motor under investigation varies in frequency, the filter system will automatically track to reject power line carrier frequency. After filtering, the remaining signal is amplified to exploit the full practical range of an analog-to-digital converter. This

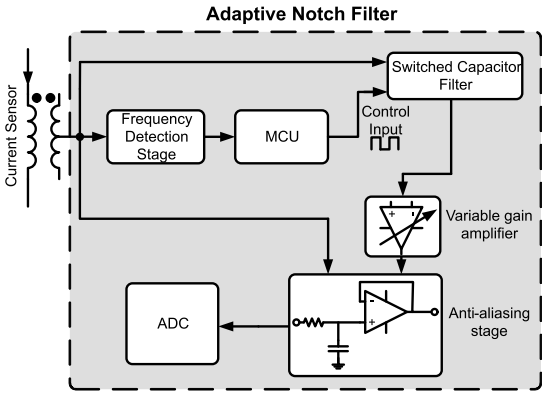

Fig. 7. Adaptive discrete-time notch filter.

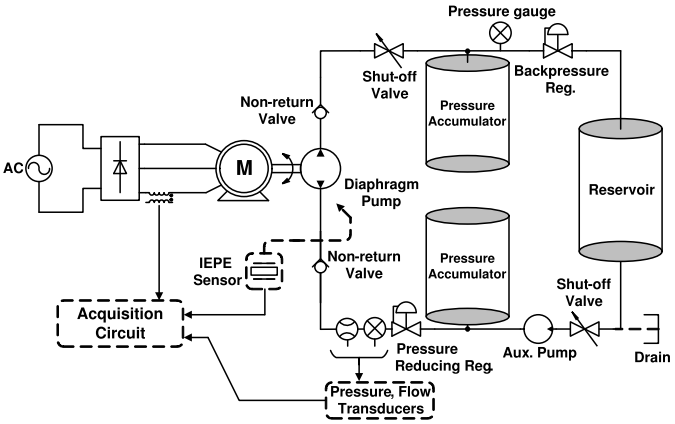

Fig. 8. Experimental setup with diaphragm pump.

maximizes the SNR [27], specifically targeting parts of the signal which contain diagnostic information.

B. Diaphragm Pump Experiment

The experimental setup, focused on a LEWA EK-1 diaphragm pump, was constructed for this study. Fig. 8 presents a schematic diagram of the setup. Inlet and outlet pressure accumulators were used together with pressure regulators to create appropriate pressure levels at the input and output of the pump. The pump is driven by a 0.5 HP, 4-pole induction motor. It features an internal gearbox with a 10:1 ratio. The pump in the setup is equipped with a nonspring loaded ball-type check valve at both the inlet and outlet ports. The diaphragm installed during the experiments was manufactured from polytetrafluoroethylene (PTFE). Table I presents physical parameters used during experiments with the setup. Volumetric flow measurements were recorded to track the time necessary to displace a fixed amount of fluid [15].

The valve clogging phenomenon was emulated by gradually clogging the inlet check valve by means of a strong hydraulic sealant. Fig. 9 shows different stages in the clogging process, and the check valve bracket and ball are visible. In order to analyze the results presented in Section IV, we introduce a figure-of-merit, the "clogging stage." The clogging stage is an empirical quantity that describes the percentage of the valve opening that has been clogged.

TABLE I
SETUP DETAILS

Parameter:	Range:
Output pressure,[psi]	60-185
Input pressure,[psi]	40
Flow,[l/min]	0-4
Temperature, [°C]	20
Viscosity, [cSt]	46(max)

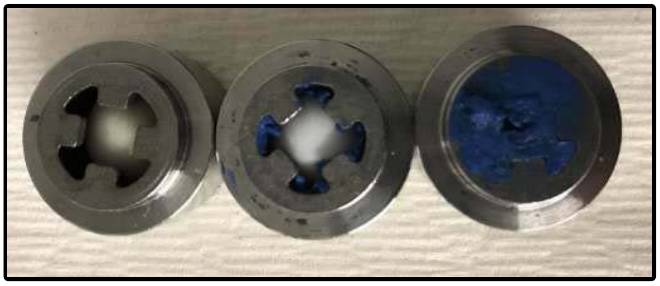

Fig. 9. Inlet valve clogging. Increasing clogging is presented starting from the left side.

Fig. 10. Fixture for diaphragm damaging.

A special fixture was machined to permit accelerated diaphragm degradation consistent with that observed in the field. The fixture in Fig. 10 allows the application of force perpendicular to the membrane. The value of the force was empirically adjusted. The specific results presented in Section IV correspond to a membrane stretched with 800-N force, which emulates damage that might be experienced by the diaphragm during a malfunction.

IV. EXPERIMENTAL RESULTS

The performance of the proposed diagnostic techniques is demonstrated in this section. Acquired data were sampled at 21 kHz with a 24-b resolution over a 20-s measurement interval during pump operation. The MES values were obtained for 0–21-kHz range. All results were obtained with a working fluid consisting of food-grade hydraulic oil with a viscosity of 46 cSt. The inlet pressure was fixed at 275.79 kPa (40 psi), while the output pressure was kept at 1172.11 kPa (170 psi).

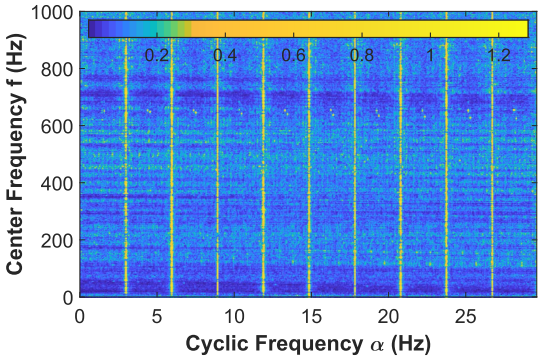

Fig. 11. Spectral coherence map for pump vibration.

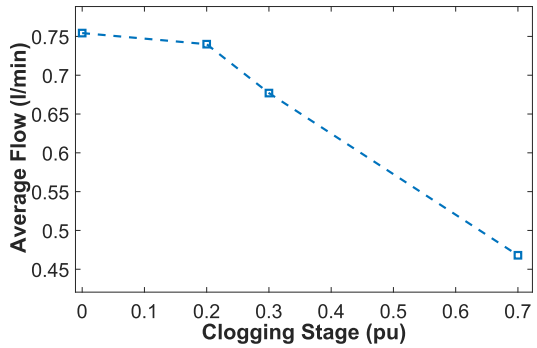

Fig. 12. Average flow as a function of the clogging stage.

A. Vibration-Based Approach

Fig. 11 presents the spectral coherence map for diaphragm pump vibration signal. Distinct vertical lines at multiples of the pumping frequency reveal significant random content in the vibration signal. This is expected for structures with multiple fluid-structure interactions and several rotating components supported with bearings and the internal gear. The pump operates with a *four–pole* motor connected to a utility with a 60-Hz electrical frequency. The resulting motor mechanical shaft rotation near 30 Hz passes through a 10:1 internal gear ratio to produce a reciprocating motion with frequency in the vicinity of 3 Hz, depending on the loading condition and slip value. Detection of cyclostationary components provides clear indication of the existing modulation frequencies and spectral location of the carrier frequencies.

1) Valve Clogging: A first approach uses the cyclostationary content of the vibration signal to detect the valve clogging phenomenon. Progressive clogging of the inlet valve leads to a decrease in the average flow. Obviously a decrease in the flow level is an intuitive method of detection often used in the field. However, a good diagnostic tool should allow for an early indication of failure even without a significant decrease in the average flow. Fig. 12 presents a relation between the clogging stage and the measured averaged flow. It can be seen that for 20% clogging stage, the flow rate decreases slightly. However, for the severe case the flow value is only 60% of the clean case. Fig. 13 relates the value of the MES with the clogging stage. It can be seen that the indicator increases with progressing clogging. For the clogging stage of 0.3 pu, there

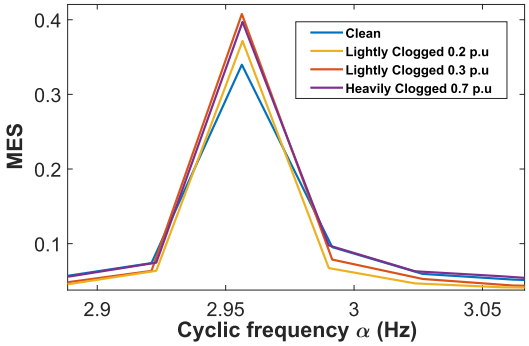

Fig. 13. MES zoomed in at fundamental cyclic frequency.

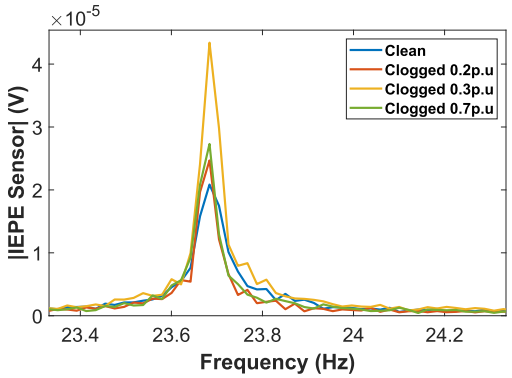

Fig. 14. Magnitude frequency spectrum of the IEPE sensor reading.

Fig. 15. Reverse emulation of the clogging process.

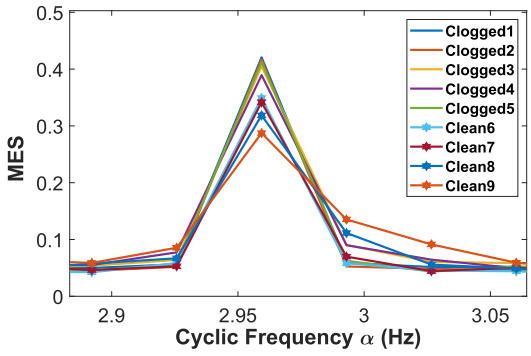

Fig. 16. MES during experiment.

is a clear increase in the MES, as compared with a clean case. Contrastingly, the average flow at the same stage is about 90% of the clean case. This is a promising performance from the condition monitoring point of view.

The second quantity used for the assessment of the valve condition is energy present at the resonant frequency. This is shown in Fig. 14. For low clogging stages, the flow volume is essentially similar. This means that, for a fixed amount of fluid and a smaller available check valve area, the average speed of the working fluid increases. The increase in the average speed results in higher magnitude values of spectral content near the resonance, exciting monotonically increasing vibration levels with clogging. For heavier clogs, e.g., a 0.7-pu clogging stage, flow volume is substantially impacted as the flow value drops by more than 40%. That is, as clogging becomes heavier, the trend in vibration energy will reverse.

A clear increase in the value of both the MES and energy at the resonant frequency can be observed for low clogging stages, i.e., for which the flow is maintained above 90% of its initial value. Clogging is a gradual process of filling openings in the valve bracket, and early clogging stages can be reliably detected by both methods. Consequently, the nonmonotonic behavior for severe clogging does not discount or eliminate the value of either of the diagnostic indicators as a clog develops. Each result presented in Figs. 13 and 14 is the average of ten data sets acquired independently.

In an industrial environment, clogging increases gradually depending on the solid fraction of the pumping fluid, its viscosity, and other factors. Continuous operation of the experimental setup and addition of impurities in laboratory conditions is very difficult. Here, we emulate this situation by reversing the process. The hydraulic sealant used for clogging emulation presented good endurance in providing a clog. However, long operation at constant input and output pressures can lead to the gradual removal of the sealing insert from the valve bracket. Starting with the clogging stage of approximately 0.3 pu, the pump was being operated until the desired clearing or removal of the sealant clog was achieved. This test technique facilitates recording measurements for different valve conditions without physical intervention into the pump's mechanism, ensuring an operating cycle that is consistent with sustained use in an industrial environment. Fig. 15 shows gradual removal of the sealant clog over the course of an experimental cycle (compare with Fig. 9 to see the effect). Fig. 16 presents the MES, and Fig. 17 presents a peak of the magnitude frequency spectrum near the resonant frequency. Data sets directly before and after the sealant removal were recorded. The measurements are presented in a chronological order as labeled in the legends. In Fig. 16, the evolution of the cleaning process is visible. There is a clear change in the MES value when comparing the data set labeled as Clean6 with the previous measurements. This is where significant weakening of the sealant structure happened. Further measurements Clean7–Clean9 present how this process evolved and led to the state presented in Fig. 15. Fig. 17 shows peak values of the magnitude spectrum at the resonant frequency, represented as a bar plot for clarity. As the sealant removal progresses, a decreasing trend in the peak energy at the resonant frequency can be observed. Both of

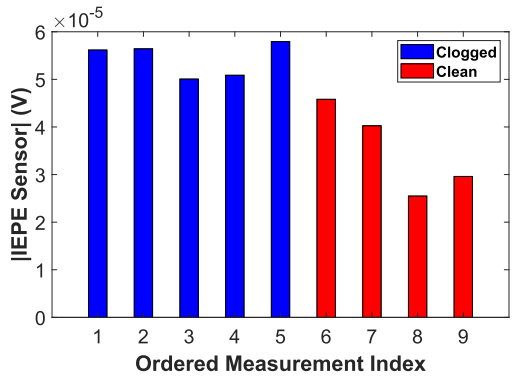

Fig. 17. Resonant peak of magnitude frequency spectrum of the sensor reading.

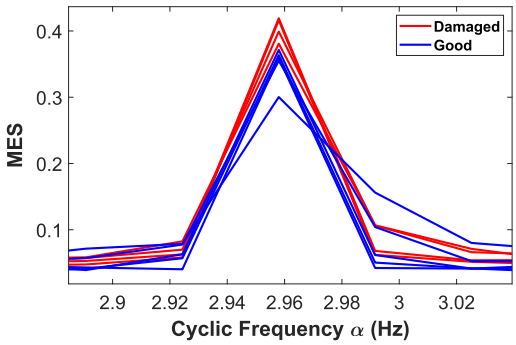

Fig. 18. MES for good and damaged diaphragms.

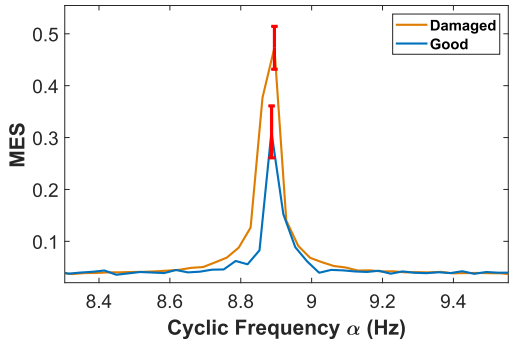

Fig. 19. MES evaluated at the third harmonic.

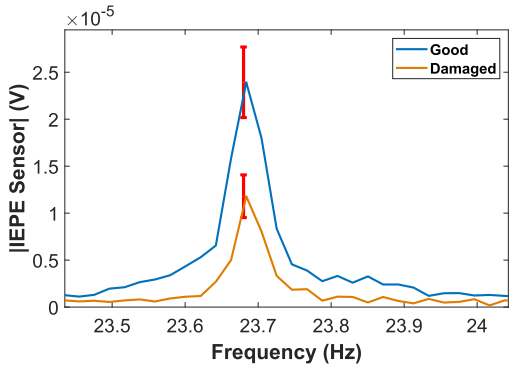

Fig. 20. Magnitude frequency spectrum for different diaphragms.

the applied techniques are able to detect a change in the valve condition. Especially, the MES-based approach presents a clean and valuable condition indicator.

2) Diaphragm Degradation: The second phenomenon targeted in this article searches for diaphragm degradation. The performance of two diaphragms was compared, a new PTFE diaphragm and one stressed as described in Section III. Both the MES and energy at the resonant frequency approaches are tested. Fig. 18 presents the value of the MES for both diaphragms. Five independent measurement sets are presented for both cases. An increase in the value of the MES at the fundamental cyclic frequency can be noticed for a damaged diaphragm case. However, it is not as pronounced as for the valve clogging problem. Inspection of Fig. 11 reveals that there is significant energy at multiple harmonics of the fundamental cyclic frequency α. Indeed, the third harmonic of α presents a good indication and allows for distinction between both diaphragms, as shown in Fig. 19. Error bars represent the standard deviation across five independent measurement sets.

While there is no *a priori* reason to choose any particular harmonic sideband as the diagnostic indicator, we have observed several practical approaches to developing a diagnostic metric from the frequency data. First, a composite indicator can be found that sums content across many sidebands. Second, we have found that the choice of any particular sideband is not critical, as the diaphragm excites a broad set of sideband modulations. In particular installations, it is conceivable that the metric is best determined by examining trends over a period of operating life.

In addition, we note that the machine may offer an obvious choice of frequency for developing a diagnostic metric: a natural resonance of the mechanical structure, which amplifies the effect of the changes. Fig. 20 compares the magnitude frequency spectra zoomed in at the resonant frequency. It can be seen that the condition of diaphragm significantly contributes to the way the resonance is excited. The damaged diaphragm is substantially less efficient in pumping, and therefore, provides less excitation at the resonant frequency. This is reflected in Fig. 20 as a *reduced* peak or energy content in the damaged condition in comparison to undamaged operation. The results in Fig. 20 are the averages of five measurement sets. Error bars represent the standard deviation of the resonant frequency peak magnitude.

B. Current-Based Approach

A current signal can also be utilized to detect diaphragm degradation and valve clogging. The current signal used in this analysis is the output of the discrete-time notch filter on the data acquisition board.

High fidelity measurements of the filtered current allow for the identification of sidebands around the fundamental frequency. Change in energy of the sideband frequencies is utilized to monitor the device under study. Fig. 21 shows the fifth sideband of the fundamental 3-Hz modulation. Similarly, as in Section IV-A, the presented data are an average of five data sets. Error bars represent the standard deviation

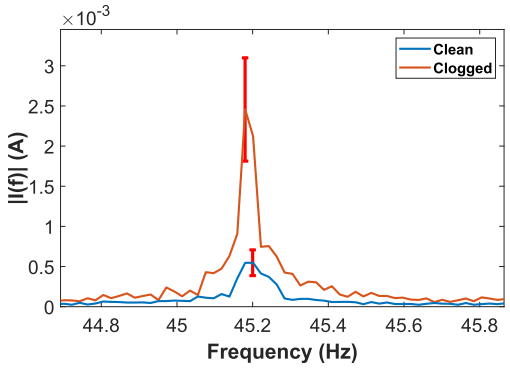

Fig. 21. Comparison of current frequency spectra, valve clogging.

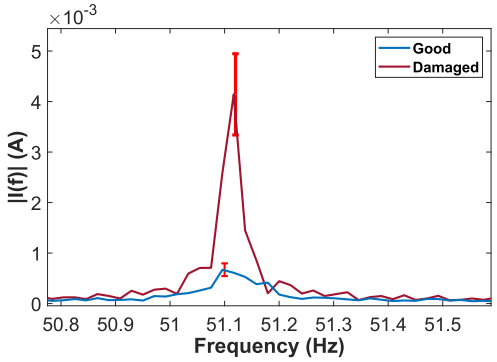

Fig. 22. Comparison of current frequency spectra, diaphragm degradation.

of the magnitude spectrum peak value. A clear indication of progressing clogging is observed. Consequently, it can be concluded that monitoring of the energy levels at this frequency could be used as a detection tool. There is a significant increase in the variance of the current sidebands for the clogged case as shown in Fig. 21.

A similar approach will detect diaphragm degradation. In this case, the third sideband was identified as a strong signal for use as a diagnostic indicator. In general, the amplitudes of the sidebands will vary with the mechanical system and the electric machine and should be chosen to provide the largest signal for diagnostic detection. Fig. 22 presents the magnitude spectrum located around the third sideband. In this case, the change in the average value of a given frequency component is even higher than for the valve clogging scenario. Current signal analysis in the frequency domain allows to successfully detect the problems of interest.

V. Conclusion

Two low-intrusive diagnostic tools are presented in this article. The first one relies on the acceleration data. Monitoring of cyclostationary components with the MES in an acceleration signal was applied as a candidate method and proved to be a solid diagnostic tool. The experimental results showed that it can successfully monitor valve and diaphragm condition despite the complex mechanical structure of the device under study. It presented a superior performance for signals where periodic modulations interfere with essentially random content. Such a scenario is common for a wide range of industrial actuators with a diaphragm pump being a good example. In addition, the energy of the vibration signal at the mechanical resonant frequency was successfully deployed for condition monitoring. The second approach is based on the analysis of the frequency content in the current signal. Adaptive discrete-time notch filter allowed for optimal analog-to-digital conversion of the signal of interest. Two frequency locations were identified as candidates for detection of the valve clogging and diaphragm degradation phenomena.

The approach presented in this article and verified on a diaphragm pump case can be generalized to a broader class of devices. The MES indicator relies on the detection of hidden periodicity in a vibration signal, and hence, can be applied for all electromechanical, pneumatic, or hydraulic actuators driving periodic loads. Similarly, monitoring of the energy at the device-specific mechanical resonant frequency can be applied to a broad class of devices. Analysis of the current signal in the frequency domain targets specifically devices driven by electric machines; however, it presents a great low-intrusive monitoring tool.

Appendix

Given a discrete-time signal $x(t_n)$, the spectral correlation function for the discrete-time case is given as

$$S_x(\alpha, f) = \lim_{N\to\infty} \frac{1}{(2N+1)F_s} \sum_{n=-N}^{n=N} \sum_{m=-\infty}^{m=+\infty} \times [R_x(t_n, \tau_m) e^{-j2\pi n \frac{\alpha}{F_s}} e^{-j2\pi m \frac{f}{F_s}}] \quad (10)$$

where F_s is sampling frequency, α is a cyclic frequency, f is a carrier frequency, $t_n = (n/F_s)$, $\tau_m = (m/F_s)$, and $R_x(t_n, \tau_m)$ is an autocorrelation function of $x(t_n)$.

References

[1] C. G. Dias and I. E. Chabu, "Spectral analysis using a Hall effect sensor for diagnosing broken bars in large induction motors," *IEEE Trans. Instrum. Meas.*, vol. 63, no. 12, pp. 2890–2902, Dec. 2014.

[2] X. Xu, M. Zhao, J. Lin, and Y. Lei, "Envelope harmonic-to-noise ratio for periodic impulses detection and its application to bearing diagnosis," *Measurement*, vol. 91, pp. 385–397, Sep. 2016. [Online]. Available: http://www.sciencedirect.com/science/article/pii/S0263224116302408

[3] L. Cristaldi, M. Faifer, M. Lazzaroni, and S. Toscani, "An inverter-fed induction motor diagnostic tool based on time-domain current analysis," *IEEE Trans. Instrum. Meas.*, vol. 58, no. 5, pp. 1454–1461, May 2009.

[4] J. Antoni, "Cyclostationarity by examples," *Mech. Syst. Signal Process.*, vol. 23, no. 4, pp. 987–1036, May 2009. [Online]. Available: http://www.sciencedirect.com/science/article/pii/S0888327008002690

[5] M. Ahmed, A. Smith, F. Gu, and A. D. Ball, "Fault diagnosis of reciprocating compressors using revelance vector machines with a genetic algorithm based on vibration data," in *Proc. 20th Int. Conf. Automat. Comput.*, Sep. 2014, pp. 164–169.

[6] C. J. Schantz and S. B. Leeb, "Self-sensing induction motors for condition monitoring," *IEEE Sensors J.*, vol. 17, no. 12, pp. 3735–3743, Jun. 2017.

[7] J. Zhang, Y. Chang, and Z. Xing, "Study on self-sensor of linear moving magnet compressor's piston stroke," *IEEE Sensors J.*, vol. 9, no. 2, pp. 154–158, Feb. 2009.

[8] Z. Zhao, S. Wu, B. Qiao, S. Wang, and X. Chen, "Enhanced sparse period-group lasso for bearing fault diagnosis," *IEEE Trans. Ind. Electron.*, vol. 66, no. 3, pp. 2143–2153, Mar. 2019.

[9] G. Betta, C. Liguori, A. Paolillo, and A. Pietrosanto, "A DSP-based FFT-analyzer for the fault diagnosis of rotating machine based on vibration analysis," *IEEE Trans. Instrum. Meas.*, vol. 51, no. 6, pp. 1316–1322, Dec. 2002.

[10] J. Antoni, "Cyclic spectral analysis of rolling-element bearing signals: Facts and fictions," *J. Sound Vibrat.*, vol. 304, nos. 3–5, pp. 497–529, 2017. [Online]. Available: http://www.sciencedirect.com/science/article/pii/S0022460X07001551
[11] Y. Soleimani, S. M. A. Cruz, and F. Haghjoo, "Broken rotor bar detection in induction motors based on air-gap rotational magnetic field measurement," *IEEE Trans. Instrum. Meas.*, vol. 68, no. 8, pp. 2916–2925, Aug. 2019.
[12] Y. Hong, M. Kim, H. Lee, J. J. Park, and D. Lee, "Early fault diagnosis and classification of ball bearing using enhanced kurtogram and Gaussian mixture model," *IEEE Trans. Instrum. Meas.*, to be published.
[13] X.-Q. Ling, Y.-L. Zhang, and W. Zhang, "Design of optimization of diaphragm chamber based on finite element method," in *Proc. Int. Conf. Comput. Intell. Commun. Netw. (CICN)*, Dec. 2015, pp. 627–629.
[14] V. Kroumov and Y. Kobayashi, "Development and control of a novel type diaphragm pump using a DSP," in *Proc. Int. Conf. Adv. Mech. Syst.*, Sep. 2012, pp. 98–103.
[15] M. B. Alberto, F. O. J. Manuel, and M. F. Andrés, "Numerical methodology for the CFD simulation of diaphragm volumetric pumps," *Int. J. Mech. Sci.*, vol. 150, pp. 322–336, Jan. 2019. [Online]. Available: http://www.sciencedirect.com/science/article/pii/S002074031830242X
[16] *LEWA Operating Handbook, B 0.050*. Leonberg, Germany, LEWA GmbH, 1998.
[17] R. van Rijswick, A. Talmon, and C. van Rhee, "Fluid structure interaction (FSI) in piston diaphragm pumps," *Can. J. Chem. Eng.*, vol. 94, no. 6, pp. 1116–1126, 2016. [Online]. Available: https://onlinelibrary.wiley.com/doi/abs/10.1002/cjce.22487
[18] R. Ciocan and N. Ida, "Method of early failure detection for elastic diaphragms based on frequency analysis of the acoustic signal," *IEEE Trans. Ultrason., Ferroelectr., Freq. Control*, vol. 49, no. 8, pp. 1025–1028, Aug. 2002.
[19] J. H. Powell and J. H. T. Roberts, "On the frequency of vibration of circular diaphragms," *Proc. Phys. Soc. London*, vol. 35, p. 170, Jan. 1923.
[20] F. He and W. Shi, "WPT-SVMs based approach for fault detection of valves in reciprocating pumps," in *Proc. Amer. Control Conf.*, vol. 6, May 2002, pp. 4566–4570.
[21] *Lewa Catalogue*. Accessed: 2000. [Online]. Available: http://www.lewa-inc.com
[22] F. Griffiths and M. Ooi, "The fourth industrial revolution—Industry 4.0 and IoT [Trends in Future I&M]," *IEEE Instrum. Meas. Mag.*, vol. 21, no. 6, pp. 29–43, Dec. 2018.
[23] W. A. Gardner, *Introduction to Random Processes with Applications to Signals and Systems*. New York, NY, USA: Macmillan, 1986.
[24] W. Gardner, "Measurement of spectral correlation," *IEEE Trans. Acoust., Speech, Signal Process.*, vol. ASSP-34, no. 5, pp. 1111–1123, Oct. 1986.
[25] J. Antoni, "Cyclic spectral analysis in practice," *Mech. Syst. Signal Process.*, vol. 21, no. 2, pp. 597–630, Feb. 2007. [Online]. Available: http://www.sciencedirect.com/science/article/pii/S0888327006001816
[26] J. Antoni, G. Xin, and N. Hamzaoui, "Fast computation of the spectral correlation," *Mech. Syst. Signal Process.*, vol. 92, pp. 248–277, Aug. 2017. [Online]. Available: http://www.sciencedirect.com/science/article/pii/S0888327017300134
[27] A. V. Oppenheim and R. W. Schafer, *Discrete Time Signal Processing*. London, U.K.: Pearson, 2013.
[28] W. A. Gardner, "The spectral correlation theory of cyclostationary time-series," *Signal Process.*, vol. 11, no. 1, pp. 13–36, 1986. [Online]. Available: http://www.sciencedirect.com/science/article/pii/0165168486900927
[29] J. Antoni. (Dec. 2016). *Fast Spectral Correlation*. [Online]. Available: https://www.mathworks.com

Łukasz Huchel received the B.Sc. degree in electrical power engineering from the Silesian University of Technology, Gliwice, Poland, in 2013, and the M.Sc. degree from the Department of Electrical Engineering and Computer Science (EECS), Masdar Institute of Science and Technology, Abu Dhabi, United Arab Emirates, in 2015. He is currently pursuing the Ph.D. degree in EECS with the Massachusetts Institute of Technology, Cambridge, MA, USA.

His current research interests include the development of signal processing algorithms, and hardware and software solutions for condition monitoring and diagnostics.

Jan Helsen received the M.Sc. degree in electromechanical engineering and the Ph.D. degree from Katholieke Universiteit Leuven, Leuven, Belgium, in 2007 and 2012, respectively. His Ph.D. thesis was focused on the dynamic simulation of wind turbine gearboxes.

He is currently a Professor with the Acoustics and Vibrations Research Group, Vrije Universiteit Brussel, Brussel, Belgium. His current research interest includes condition monitoring of rotating systems.

Peter A. Lindahl received the B.S. degree in electrical engineering from Penn State University, State College, PA, USA, in 2003, and the M.S. degree in electrical engineering and the Ph.D. degree in engineering from Montana State University, Bozeman, MT, USA, in 2009 and 2013, respectively.

He joined as a Post-Doctoral Associate with the Research Laboratory of Electronics, Massachusetts Institute of Technology, Cambridge, MA, USA, in 2014. He is currently a Senior Associate in the electrical engineering and computer science practice with Exponent, Inc., where he provides technical consulting services regarding energy and power systems, electromechanical machinery, sensors and instrumentation, and industrial controls.

Steven B. Leeb received the Ph.D. degree in electrical engineering and computer science from the Massachusetts Institute of Technology (MIT), Cambridge, MA, USA, in 1993.

Since 1993, he has been a Faculty Member with the Department of Electrical Engineering and Computer Science, MIT, where he also holds a joint appointment with the Department of Mechanical Engineering. His current research interests include the development of signal processing algorithms for energy and real-time control applications.